Universality class of the structural phase transition in the normal phase of cuprate superconductors

M. N. Najafi and A. Tavana
Department of Physics, University of Mohaghegh Ardabili, P.O. Box 179, Ardabil, Iran
(Received 15 March 2016; revised manuscript received 19 June 2016; published 8 August 2016)

The tetragonal-orthorhombic structural phase transition of oxygen atoms in the basal plane of $YBa_2Cu_3O_{6+\delta}$ high-T_C cuprate superconductors is studied numerically. By mapping the system onto the asymmetric next-nearest-neighbor Ising model, we characterize this phase transition. Results indicate the degrees of critical behavior. We show that this phase transition occurs at the temperature $T_C \simeq 0.148$ eV in the thermodynamic limit. By analyzing the critical exponents, it is found that this universality class displays some common features, with the two-dimensional three-state Potts model universality class, although the possibility of other universality classes cannot be ruled out. Conformal invariance at $T = T_c$ is investigated using the Schramm-Loewner evolution (SLE) technique, and it is found that the SLE diffusivity parameter for this system is 3.34 ± 0.01.

DOI: 10.1103/PhysRevE.94.022110

I. INTRODUCTION

Unconventional superconductivity remains a challenging problem in low-temperature physics. Copper oxide superconductors have very rich electronic and structural phase diagrams, incorporating signatures of different physical phenomena, which result in different competing orders. In these materials, superconductivity appears in proximity or in competition with symmetry-breaking in the ground state [1]. Optimal doping seems to occur near a quantum phase transition of magnetic ordering [2], while at the same time, a strong isotope effect of the oxygen atoms [3] or the well-known lattice instabilities [4] indicates a noticeable electron-phonon interaction in these compounds.

The Y-Ba-Cu-O family of cuprate superconductors itself consists of several family members that differ in the number of the CuO_2 planes and the CuO chains and their stacking sequence. CuO chains are the exclusive property of this family among other cuprates. These chains are believed to play the role of a carrier reservoir with a minor direct contribution in the superconductivity of the system. Holes can be doped to the CuO_2 planes by adding (removing) oxygen atoms to (from) the chains. So, all doping-dependent properties, especially superconductivity itself, should be related to the formation and ordering of these chains.

$YBa_2Cu_3O_{6+\delta}$ (Y123) is the first discovered and most studied member of this family. In Y123, at $\delta \simeq 0.4$, the antiferromagnetic order disappears and superconductivity begins simultaneously with a structural phase transition from tetragonal to orthorhombic phase. This structural symmetry reduction is related to the redistribution of the oxygen atoms in the basal plane, where the CuO chains form [5]. Numerous x-ray diffraction (XRD), nuclear magnetic resonance (NMR), and nuclear quadrupole resonance (NQR) investigations indicate the importance of oxygen ordering in the basal plane at $\delta \simeq 0.5$ [6–10]. A detailed characterization of the nature of phase transitions at this doping value can partly clarify the interplay between the lattice and the electronic properties of this family, which is scarce in the literature. In this paper, by focusing on a semiclassical model, i.e., the asymmetric next-nearest-neighbor Ising (ASYNNNI) model [11,12], we study the dynamics of oxygen atoms in the basal plane of this compound at $\delta \simeq 0.5$. Toward that end, employing the Monte Carlo (MC) and the Schramm-Loewner evolution (SLE) techniques, the oxygen ordering and critical properties of the structural phase transition in the basal plane of a Y123 superconductor are investigated. This model is partly able to address some properties of this compound, e.g., the plateau problem [13] or the structural phase formations. The parameters of the ASYNNNI model are calculated by means of *ab initio* density-functional theory (DFT). Two kinds of statistical quantities are analyzed in this paper to characterize the transition, namely the local and the global quantities. We show that thermodynamic quantities exhibit sharply singular behavior at the critical temperature. The exponents of these quantities in the critical region are reported as a function of system size. The most important global (geometrical) quantity in our analysis is the fractal dimension of the exterior perimeter of the geometrical spin clusters. We present a complete analysis of these critical loops defined in the model, e.g., their gyration radius, loop length, and cluster mass. Finite-size arguments help us to determine the exponents in the thermodynamic limit. In the second part, we address the conformal invariance of the model right at the critical temperature. We analyze (boundary-to-boundary) conformal curves using the SLE technique, which aims to classify two-dimensional (2D) critical models into some one-parameter universality classes. To be more precise, we employ two methods to apply the SLE formalism: the strip-compatible SLE, and the SLE(κ, ρ), which is a variant of the SLE theory. The results show degrees of similarities with the three-state Potts model, as well as the ordinary Ising model. The paper has been organized as follows: In Sec. II, we introduce the physics of the system and its relation to the ASYNNNI model. Section III is devoted to the numerical details, and the calculated local exponents are analyzed and discussed in Sec. IV. Geometrical aspects of the ASYNNNI model are investigated in Sec. V. Section VI is devoted to the SLE and conformal invariance of the interfaces of the model at hand.

II. PHYSICS OF THE T-OII TRANSITION

The unit cell of the Y123 compound has been schematically depicted in Fig. 1. Y123 has two symmetrically equivalent CuO_2 planes and one CuO chain in the basal plane. For

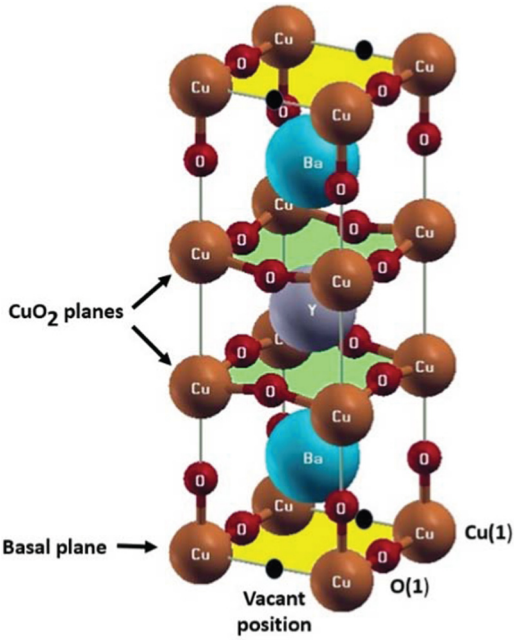

FIG. 1. Building blocks of YBCO structure.

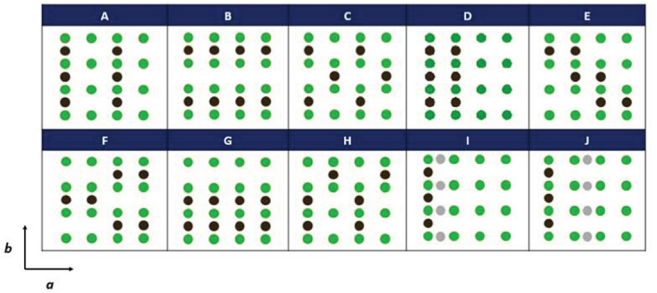

FIG. 2. The ten considered oxygen configurations. Black (green) solid circles are oxygen (copper) atoms.

$\delta < 0.4$, oxygen atoms are almost randomly distributed in the basal plane and only a few long enough, randomly oriented CuO chains may form. So, there is no noticeable difference between the lattice parameters a and b, and the symmetry is tetragonal. For higher doping concentrations, many long parallel CuO chains begin to form, resulting in the orthorhombic phases. According to the doping concentration, the stacking sequence of the chains differs, and different orthorhombic phases may appear [5]. One orthorhombic phase is the OII phase, in which the CuO chains have a staggered configuration and the distance between two successive parallel chains is equal to two-lattice parameters perpendicular to the chain direction. The other important orthorhombic phase is the so called OI phase, in which long parallel chains exist with one-lattice parameter separation. This phase is stable at low temperatures for $\delta = 1$. At $\delta = 0.5$, a tetragonal to OII phase transition is possible with temperature. Since the tetragonal-orthorhombic (T-OII) transition is believed to be a second-order transition, power-law behaviors are expected to occur with some universal exponents that determine its presumably critical universality class. The nature of this structural phase transition is diffusional, and it is expected to occur at temperatures comparable to the melting point [14].

In Y123, the detailed relationship between oxygen concentration, oxygen ordering in the basal plane, and hole doping in the CuO_2 planes is not understood, yet. Experimental evidence has revealed that the formation of nanosized striped puddles of OII phase in the basal plane, constituted from CuO chains with more than $\sim$10–13 oxygen atoms when $\delta \geqslant 0.5$, is responsible for the appearance of superconductivity [6,7]. Characterization of the T-OII transition is ambiguous when directly working out with zero-temperature *ab initio* calculations. The main issue is how to undertake the dynamics of the oxygen atoms and electrons, simultaneously. One way out of this problem is to downfold the original problem on a model Hamiltonian, which mimics the major part of the particle-particle interactions and can be used later in the simulation of that compound by MC methods. Toward that end, based on the adiabatic approximation, the kinetic energy of oxygen ions is ignored. Then, we are left with the so-called electronic adiabatic Hamiltonian to be handled by means of DFT. Since the dynamics of oxygen ions are very slow compared with electrons, and the system is being analyzed at finite temperatures, the oxygen atom dynamics can be considered to be classic. Based on the occupation of each lattice site i with oxygen atoms, we have two degrees of freedom: empty, i.e., $|0\rangle_i$, or occupied, i.e., $|1\rangle_i$. So, one can adjust a *pseudospin* variable to each site. Based on these pseudospin variables, in the OII phase the ordering is ferromagnetic in one direction and antiferromagnetic in the perpendicular direction. In this phase, we can define the staggered spin in which the spin of, say, even columns (chains in the y direction) is flipped, i.e., $s_{\text{stag}}(i,j) \equiv (-1)^i s(i,j)$, in which i and j show components perpendicular and parallel to the chains, respectively, in the square lattice. Therefore, in the tetragonal phase, $M_{\text{stag}} \equiv \langle s_{\text{stag}} \rangle = 0$, whereas for the OII phase this quantity begins to grow as a function of temperature. This *order parameter* is analyzed in this paper. We show that M_{stag}, as well as C_v, shows sharp singular behavior at the critical temperature. The SLE technique is also employed to analyze the critical staggered spin-domain walls of the ASYNNNI model.

III. METHOD AND COMPUTATIONAL DETAILS

Using DFT, we can calculate the ground-state energy of the YBCO unit cell for each oxygen configuration in the basal plane, and then from the cluster expansion of pair interactions, the coupling constants, J_{ij}, of the Ising-like ASYNNNI model ($H = -\sum_{j>i} J_{ij} s_i s_j$) can be determined. For this, the energy per unit cell of the ten most stable configurations (Fig. 2) is calculated, and then it is set equal to the corresponding expansions derived from the model Hamiltonian. This yields the coupling constants of the ASYNNNI model, with reasonable accuracy. From the obtained values, it is found that the interaction of an oxygen atom placed between two vertically successive Cu atoms (a vertical site) and another O atom placed between two horizontally successive Cu atoms (a horizontal site) is negligibly small. This is the case for every other interaction between two oxygen atoms, one at a vertical and the other at a horizontal site (e.g., see Fig. 2, C and J). In practice, small coupling parameters between these two sublattices means that

in a local neighborhood where all oxygen atoms are located, say vertical sites, there will be a noticeable energy penalty for placing an oxygen atom at a horizontal site. This implies that the phases of vertically oriented and horizontally oriented chains should be regionally separated. So, we reconstruct our model, restricted only to one sublattice site with the corresponding interactions, assuming that the dynamics of oxygen atoms are restricted only to horizontal or vertical sites. Experiment also provides evidence that exciting oxygen ions by electron bombardments instigates the collective hopping of oxygen atoms either from a horizontal site to a vacant vertical chain site or by reshuffling the chain segments to extend the average length of chains without changing the overall oxygen content [15].

Based on the ASYNNNI model, one obtains phase-formation temperatures that are much higher than room temperature. It is an accepted opinion that the room-temperature phase is a frozen-in structure from higher temperatures because of the small diffusivity of oxygen atoms in the perpendicular direction to the chains in this compound [10].

DFT calculations are performed using the WIEN2K code [16]. The employed basis set is linearized augmented plane waves plus local orbitals (LAPW+LO). The initial lattice parameters have been set from experiment and then have been relaxed for every structure. The muffin-tin radii have been set equal to 2.35, 2.5, 1.75, and 1.55 for Y, Ba, Cu, and O atoms, respectively. The generalized gradient approximation with Perdew-Burke-Ernzerhof (PBE) parametrizations has been used for the exchange and correlation functional. The energy separation between the core and valence states has been set equal to 6.0 Ry. The APW+LO basis set has been selected for the d orbitals of Cu atoms to have a more effective convergence. For all other atomic orbitals, we have used the LAPW basis set. The $RK_{\max}$, $L_{\max}$, and $G_{\max}$ parameters have been set equal to 7.0, 10, and 14, respectively. The number of k points in the irreducible Brillouin zone is set to 72, for which the energies are converged up to 0.0001 Ry. For supercell structures, the density of k points in the reciprocal lattice is preserved. Calculated coupling constants are reported in Fig. 3,

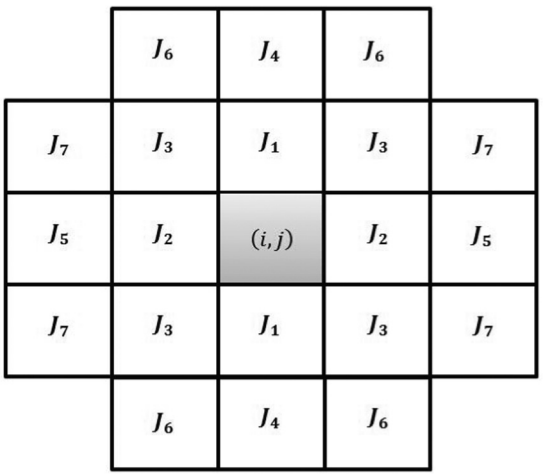

FIG. 3. The coupling constants of the ASYNNNI model. The values are as follows (in eV): $J_1 = 0.119$, $J_2 = -0.014$, $J_3 = 0.001$, $J_4 = 0.021$, $J_5 = 0.006$, $J_6 = 0.0004$, and $J_7 = 0.002$.

which shows schematically how we label different coupling parameters. In this figure, the set of sites interacting with the typical site (i, j) have been shown. The ASYNNNI model is strongly anisotropic, e.g., the first-neighbor coupling in the x direction [the coupling to the sites $(i+1, j)$ and $(i-1, j)$] J_2 and the first-neighbor coupling in the y direction [the coupling to the sites $(i, j+1)$ and $(i, j-1)$] J_1 are very different. In fact, in the x direction the coupling (J_2) is antiferromagnetic, whereas for the y direction the coupling (J_1) is ferromagnetic and $|J_1| \gg |J_2|$.

MC simulations are performed on $L \times L$ square lattices with $L = 32$, 64, 80, 100, 128, 150, 180, 256, 350, 512, and 700 and for various temperatures. Periodic boundary conditions are considered in both directions. We employ the METROPOLIS algorithm to solve the model at high and low temperatures, and in the vicinity of the critical temperature, Wolff's algorithm is used to prevent critical slowing down. The movement of an oxygen atom between two sites is translated to two simultaneous spin flips in those sites in the ASYNNNI model. To preserve the total number of oxygen atoms, we employ the demon algorithm in which single spin flips are allowed conditioned with $\delta = 0.5$ each time. We extract the set of connected sites of the same spin (geometrical spin clusters) using the Hoshen-Kopelman algorithm [17] to obtain the ensemble of critical loops. Other boundary conditions may be considered to generate stochastic curves going from boundary to boundary. To obtain an independent ensemble of samples, we flip randomly $\frac{L}{4}$ sites after extracting a sample, and we let $500L^2$ MC steps be taken before the next sample is extracted. For each system size, we start the simulation from the high-temperature limit. Near the critical points, the temperature change steps are equal to 0.001. In the SLE calculations, the minimum size of the critical curve is considered to be 1024, and for the other statistical analysis all lengths have been considered. Over 10^4 spin samples are generated for each temperature, and over 10^6 critical loops are generated for the geometrical analysis. For the SLE investigations of each setup, over 2×10^4 independent samples are generated.

IV. LOCAL TRANSITION EXPONENTS

In this part of the paper, we carry out a detailed self-contained analysis of the local quantities of the model in the critical regime, i.e., in the vicinity of the T-OII transition. Note that for the sake of convenience in the simulation, in all parts of the paper *the real temperatures are* $\frac{1}{10}$ *times the reported temperatures*, i.e., T_{real} (eV) $= \frac{1}{10}$ T.

The results of critical exponent calculations are shown in Fig. 4, and the obtained values are listed in Table I. As stated above, and as is seen in Fig. 4(a), singularity occurs at some finite temperature. The dependence of T_c on the system size has been plotted in the inset graph, from which one obtains $T_c(L \to \infty) = 1.48 \pm 0.01$, which is consistent with similar studies [13,18]. To characterize the critical aspects of the model, the critical exponents should be obtained in the vicinity of the critical temperature. Care should be taken to avoid finite-size effects in determining the critical exponents. As an example, consider the correlation length $\xi(T)$. In a finite system, one expects to have $\xi = [a(T - T_c)^{\nu} + \frac{b}{L}]^{-1}$

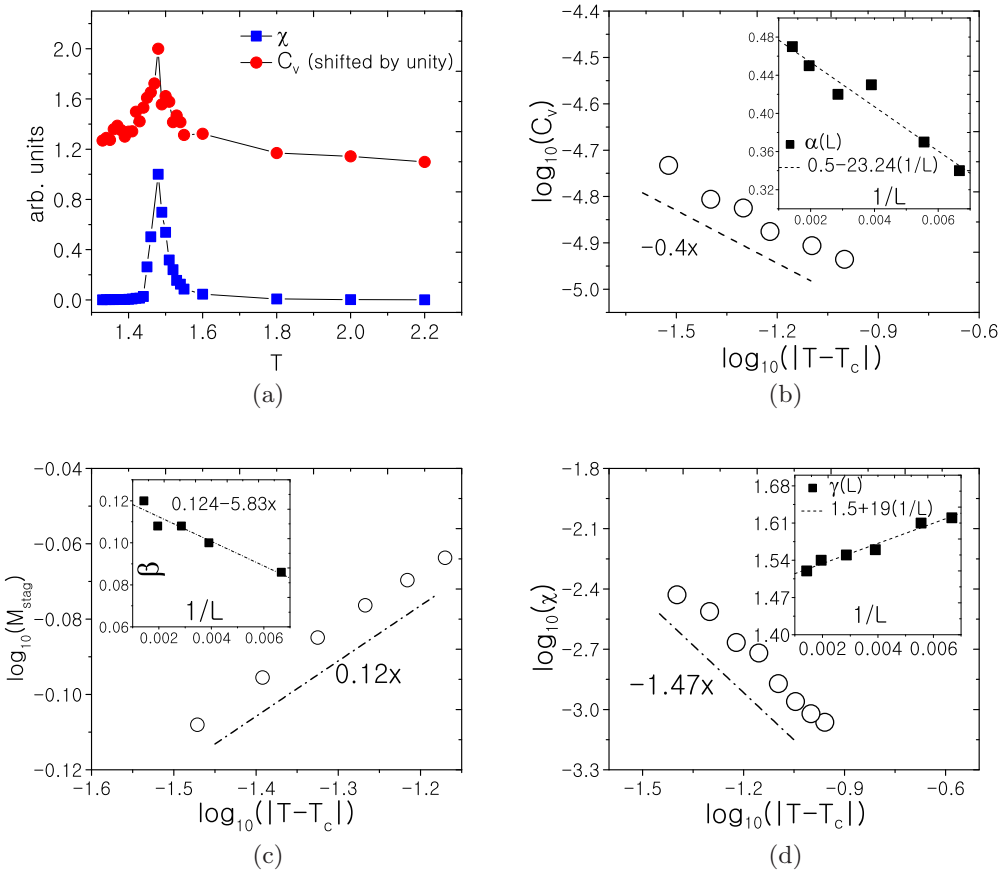

FIG. 4. (a) The singular behavior of the specific heat and the staggered susceptibility for $L = 512$. Inset: T_c as the function of system size L. (b) The log-log plot of C_v in terms of $T - T_c$. Inset: finite-size values of α. (c) The log-log plot of M_{stag} in terms of $T - T_c$. Inset: finite-size values of β. (d) The log-log plot of χ_{stag} in terms of $T - T_c$. Inset: finite-size values of γ.

(a and b are some constants), which satisfies $\xi(T_c) \sim L$ and $\xi(T, L \to \infty) \sim (T - T_c)^{-\nu}$, as expected. In many situations, the above fitting is not possible and one should find the exponent in some other way. One way is to find the linear fit of the log-log plot of ξ in terms of $T - T_c$, not very close to T_c, where the role of the term $\frac{b}{L}$ in the above formula becomes significant, and also not very far from T_c, where the power-law behavior is lost.

We fit our results with the general q-state Potts model to find the best-fitting value of q. The duality of the Potts model with other models, e.g., Coulomb gas [19], the $Z(N)$ spin model [20], the O(n) model [21], etc., helps one to acquire a deep understanding of the transition. For the q-state Potts model, the dependence of the exponents on q is as follows: the critical exponent of the heat capacity, α, defined as $C_v \sim t^{-\alpha}$, is $\alpha = 2(1 - 1/y_T)$; the critical exponent of the magnetization, β, which in our work is a staggered parameter and is defined as $M_{\text{stag}} \sim t^{\beta}$, is $\beta = (2 - y_H)/y_T$; and the critical exponent of the magnetic susceptibility, γ, defined as $\chi_{\text{stag}} \sim t^{-\gamma}$, is $\gamma = 2(y_H - 1)/y_T$. In these relations, the thermal and magnetic exponents are $y_T = 3(1 - u)/(2 - u)$ and $y_H = (3 - u)(5 - u)/4(2 - u)$, in which $0 \leqslant u \equiv (2/\pi)\cos^{-1}(\frac{\sqrt{q}}{2})$ and $t \equiv \frac{T - T_c}{T_c}$. In Figs. 4(b), 4(c), and 4(d), we have shown the critical exponents of the heat capacity, staggered magnetization, and staggered magnetic susceptibility. The exponents in the thermodynamic limit have been reported in Table I. The results are most compatible with the Ising and the three-state Potts models. For comparison, the same exponents for the Ising and the three-state Potts models have also been included in Table I. The β exponent is not distinguishable, since both the Ising and the three-state Potts models are in the error bar of the ASYNNNI model, whereas the exponents α and γ are distinguishable. A nearly clean finite-size scaling is found for all exponents, as indicated in Fig. 4.

A note is in order here: although long-range interactions can change the universality class of the Ising model [24], the interactions in the current model are actually short-range, as they involve only nearest- and next-nearest-neighbor spins, which cannot change the universality class. The second

TABLE I. The critical exponents of the three models: 2D Ising model, 2D three-state Potts model, and ASYNNNI model. The magnetic exponents of the ASYNNNI model (β and γ) have been calculated for staggered magnetization, M_{stag}. The results for the three-state Potts model have been adapted from [20,22,23].

Exponent	Definition	Ising	Three-state Potts model	ASYNNNI model
α	$C_v \sim t^{-\alpha}$	0	1/3	0.5 ± 0.1
β	$M \sim t^{\beta}$	1/8	1/9	0.11 ± 0.02
γ	$\chi \sim t^{-\gamma}$	7/4	13/9	1.50 ± 0.05

candidate for changing the universality class is anisotropy. It does change the universality class of sandpile models. In spite of this fact, extending it to equilibrium models with second-order phase transitions is, in general, conjectural.

V. GEOMETRICAL PROPERTIES OF CONFORMAL LOOPS

In this section, we present a detailed analysis of the geometrical statistical observables for the ASYNNNI model. Consider the ASYNNNI model on a square lattice in which each spin lies at the center of a square having four nearest neighbors and the spin boundaries are put on the edges of the square lattice as the dual to the original lattice. The situation has been shown in Fig. 5(a). The interfaces are defined as the separator of up and down spins inside which there may exist some other loops. Therefore, we have an ensemble of stochastic loops. In Fig. 5(b) we have shown a critical sample and a stochastic loop as the separator of the white ($s_{\text{stag}} = -1$) and the gray regions ($s_{\text{stag}} = +1$). Note that in our analysis, we consider staggered spin instead of real spins. The algorithm of extracting these stochastic loops (or the open traces, as is used in SLE analysis) is simply the so called exploration process algorithm, in which a random walker moves on the edges of the square lattice. At each step, the walker moves according to the following rule: turns left or right according to the value of the spin in front of it (for up or down, respectively). The resulting interface is a unique self-avoiding interface that can be conditioned to end on the real axis (bottom boundary) or other boundary points. Note that in the square lattice, the random walker has the choice to turn right or left, as indicated by an arrow in Fig. 5(a). In such situations, we always select the right-hand side (with respect to the previous trace, as indicated in the figure). This choice is important and affects the statistics. At $T = T_c$, these interfaces are believed to be self-affine (fractal) and can be described by the SLE in the continuum limit. At this limit, the behaviors are expected to be power-law. As an example, consider the distribution of the loop lengths, $N(l)$. In the thermodynamic limit at the critical state, one has $N(l) \sim l^{-\tau_l}$, in which τ_l is the exponent. In the finite systems, one may expect that $N(l) \sim l^{-\tau_l} F(l/L^{\gamma_{lL}})$, in which γ_{lL} is the exponent that is expected to be the fractal dimension of the loop, D_f. F is some scaling function that captures the finite-size effect of the system, having two important properties: $\lim_{x\to 0} F(x) = 1$ and $\lim_{x\to 1} F(x) = 0$. Another way to obtain the fractal dimension of the loop is to scale the loop lengths by their gyration radius r as $\langle \log(l) \rangle = D_f \langle \log(r) \rangle$.

The quantities considered in this section are the fractal dimension, D_f, the gyration radius of loops, r, loop lengths, l, and cluster masses, m. We found that at $T = T_c$, up to a scale above which the finite-size effects play the dominant role, we have $N(x) \sim x^{-\tau_x}$, in which $x = r,l,m$, and N is the corresponding distribution function. In Fig. 6, we have shown these functions. Finite-size analysis in Fig. 6(a) reveals that in the thermodynamic limit, $D_f = 1.4 \pm 0.02$. The critical state of the model is reflected in the power-law behavior of the gyration radius of loops, i.e., Fig. 6(b), in which for small length scales (with respect to the length scale at which the finite-size effects play the dominant role and the linear behavior in the log-log plot is destroyed, i.e., r_{cut}), the linear behavior in the log-log plot is evident. The corresponding exponents have been reported in Table II. The results overlap mostly with the three-state Potts model and also the Ising model. The other test for the criticality is that at $T = T_c$, the correlation length reaches the system size $\xi(T = T_c) \sim L$. A good estimation of the correlation length is r_{cut} [25]. In Fig. 6(c), we show that $r_{\text{cut}}(L)$ scales linearly with the system size L, which shows the criticality of the system. In this graph, $r_{\text{cut}}(L)$'s have been calculated as the point at which the local slope of the log-log plot, averaged over an interval around, changes considerably with respect to the mean slope up to that point.

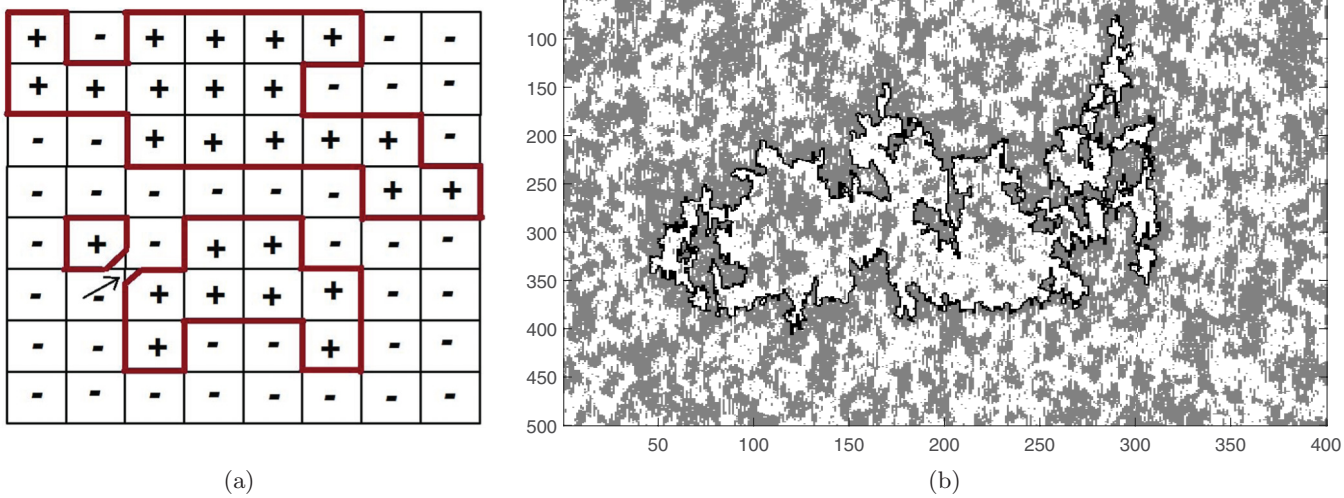

(a) (b)

FIG. 5. (a) The interfaces of the ASYNNNI system as the separator of the spin-up and spin-down sites. The interfaces can be generated by an exploration process in which one moves clockwise on the edges with the simple rule that to its right is always a (+) site and to its left is always a (−) site. A problem may arise in the configuration shown by an arrow in the figure. In these situations, the walker move to its right. (b) A staggered spin sample on the square lattice with one of its domain walls.

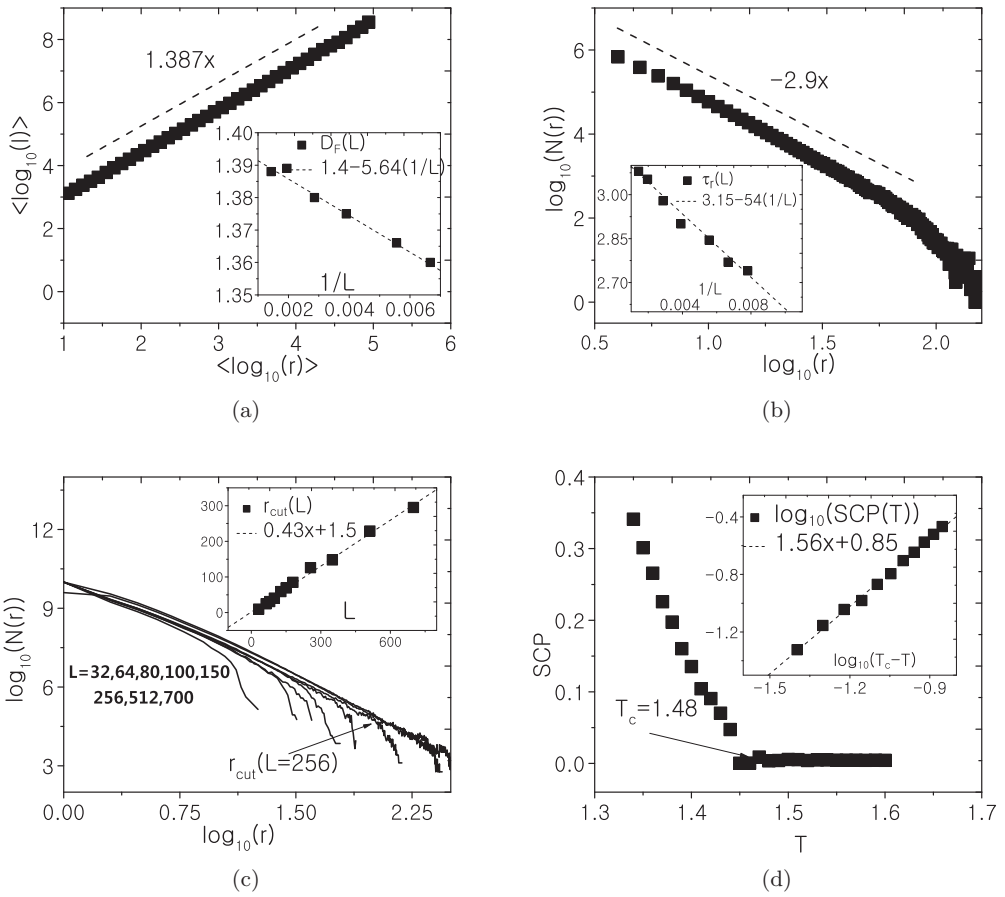

FIG. 6. (a) D_F for $L = 512$. Inset: finite-size dependence of D_F. (b) The log-log plot of $N(r)$ in terms of r. Inset: the finite-size dependence of τ_r. (c) Finite-size dependence of $N(r)$. Inset: the dependence of r_{cut} on the system size. (d) SCP in terms of temperature. Inset: Log-log plot of the SCP(T) as a function of $T_c - T$.

The Ising model may be viewed as a correlated percolation problem. For example, at $T \to \infty$ the Ising model is dual to the percolation problem [26]. Therefore, one can analyze this system as the correlated percolation problem and characterize the percolation transition in the system as a second-order transition [26]. It is shown that for the regular Ising model, this transition occurs exactly at T_c. In other words, for the percolation transition temperature, T_p, we have $T_p = T_c$ for the Ising model on the regular lattice [27]. In the ASYNNNI model, the same phenomenon is observed. Let us define the spanning cluster probability (SCP) as the probability that a randomly chosen site belongs to a spanning *staggered spin cluster* (which connects two opposite boundaries). This probability is naturally related to the temperature, SCP(T). We found that for the ASYNNNI model, the percolation transition takes place at the T-OII transition temperature, i.e., $T_p^{\text{ASYNNNI}} = T_c^{\text{ASYNNNI}}$. In Fig. 6(d), the SCP has been plotted as a function of temperature. The main result is that in the thermodynamic limit, $\text{SCP}(T < T_c, L \to \infty) \sim |t|^{\nu}$ in which $\nu = 1.56 \pm 0.1$.

TABLE II. The geometrical exponents of the ASYNNNI model (D_f, τ_x, $x = r$, l, m, and ν). The results for the three-state Potts model have been adapted from [20,22,23].

Exponent	Definition	Ising	Three-state Potts model	ASYNNNI model
D_f	$\langle \log(l) \rangle = D_f \langle \log(r) \rangle$	11/8	17/12	1.40 ± 0.02
τ_r	$N(r) \sim r^{-\tau_r}$	3.4 ± 0.1	?	3.2 ± 0.1
τ_l	$N(l) \sim r^{-\tau_l}$	27/11	41/17	2.5 ± 0.1
τ_m	$N(\text{mass}) \sim \text{mass}^{-\tau_m}$	2.3 ± 0.1	?	2.0 ± 0.1
ν	$\text{SCP}(T) \sim t^{\nu}$	?	?	1.6 ± 0.1

VI. SCHRAMM-LOEWNER EVOLUTION

The conformal symmetry at scale-invariant 2D models is shown to be very helpful to understand the lesser known models. Conformal minimal series can be considered as the other representation of universality in the critical phenomena. Therefore, fitting a lesser known model to a conformal minimal model is a valuable, albeit formidable, task in statistical analysis. Fortunately, a theory designed by Schramm [28], namely the SLE, has opened a new door in understanding the internal structure of conformal theories. In this theory, the emphasis is on the global properties of the model under study. In most statistical models, one can define some global, non-self-intersecting *interfaces*. For example, for the Ising model it can easily be defined as the separators of spin-up and spin-down sites, as defined in the previous section.

Consider a growing critical curve γ_t on the upper half-plane, i.e., $H = \{z \in \mathbb{C}, \text{Im} z \geqslant 0\}$ and $H_t := H \backslash K_t$, in which K_t is

the set of points located exactly on the γ_t trace, or disconnected from infinity by γ_t. According to Riemann mapping theorem in two dimensions, there is always a conformal mapping, $g_t(z)$, which maps $H_t \to H$, i.e., the uniformizing map, satisfying $\partial_t g_t(z) = \frac{2}{g_t(z)-\zeta_t}$ and with the initial condition $g_t(z) = z$. For the critical models, it has been shown [21,28] that ζ_t, the driving function, is a real-valued function proportional to the one-dimensional Brownian motion $\zeta_t = \sqrt{\kappa} B_t$, in which κ is known as the diffusivity parameter and $B(t)$ is one-dimensional Brownian motion. SLE aims to analyze these critical curves by classifying them into the one-parameter classes represented by κ. It is shown that the Ising model is described by SLE with the diffusivity parameter $\kappa = 3$ [21] ($c = \frac{1}{2}$CFT [29]) and for the three-state Potts model by $\kappa = 10/3$ ($c = \frac{4}{5}$CFT). For more information, see [21,28].

The method of extracting the interfaces of the model has been described in the previous section. For the SLE investigations, we generate critical stochastic curves that start from and end on the boundaries. To be more accurate, we simulate the model on two different geometries: the strip geometry and the upper half-plane geometry. Contrary to the previous sections in which the boundary conditions were considered to be periodic, in this section we consider some other boundary conditions that are compatible with the SLE.

A. Strip geometry

By mapping the Loewner equation to the strip, one can easily show that [30]

$$\frac{d}{dt} g_t^S(z) = \coth\left(\frac{g_t^S(z) - \zeta_t}{2}\right), \tag{1}$$

in which $g_t^S(z)$ is the conformal uniformizing map in the strip geometry, and $\zeta_t = \sqrt{\kappa} t$. In the discrete form for a SLE trace $\{z_0, z_1, z_2, \ldots, z_N\}$, one can solve the above equation by considering $\zeta(t_i)$ to be partially constant in the interval $[t_{i-1}, t_i)$. Then one can use the composite map $g_{t_N}^S \circ g_{t_{N-1}}^S \circ \cdots g_{t_2}^S \circ g_{t_1}^S$ to uniformize the trace step by step, in which $g_{t_i}^S(z)$ is the partial conformal map that takes the z_ith point to the real axis. It can be shown that the corresponding discrete map is [31]

$$\begin{aligned}
\Delta_i &= \mathrm{Im}\left[\frac{\pi z_i^{i-1}}{2L}\right], \quad t_i = t_{i-1} - 2(L/\pi)^2 \log[\cos(\Delta_i)], \\
\zeta(t_i) &= \mathrm{Re}\left(z_i^{i-1}\right), \\
z_j^i &= \zeta(t_i) + \frac{2L}{\pi} \cosh^{-1} \\
&\quad \times \left\{ \cosh\left[\frac{\pi\left[z_j^{i-1} - \zeta(t_i)\right]}{2L}\right] \Big/ \cos(\Delta_i) \right\},
\end{aligned} \tag{2}$$

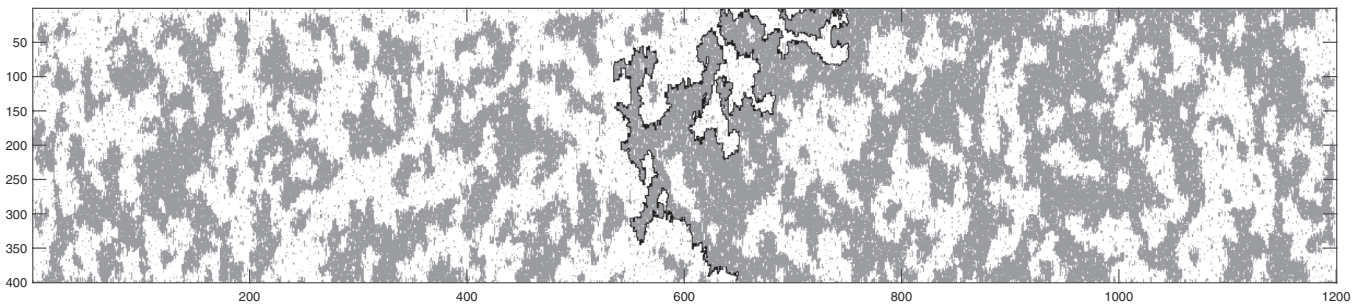

(a)

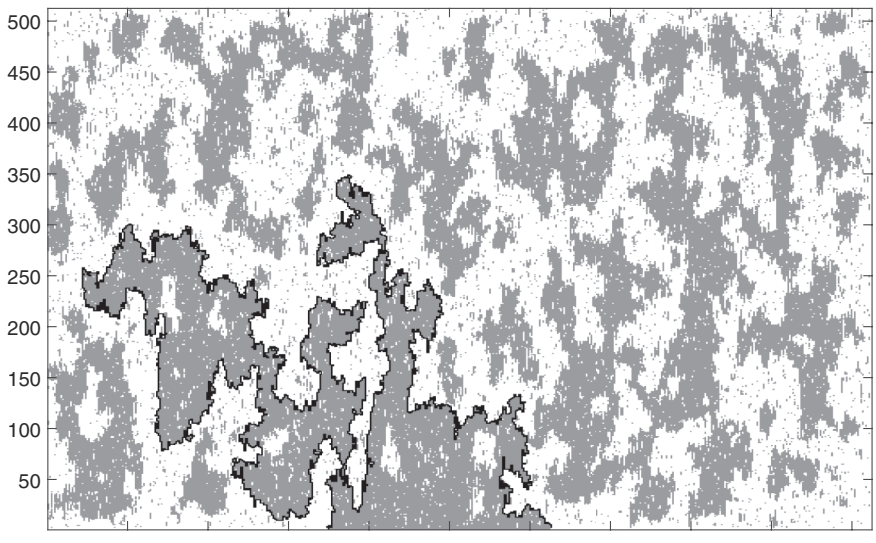

(b)

FIG. 7. Staggered spin sample with a highlighted interface on the (a) strip (1200 × 400) and (b) square (512 × 512) lattices.

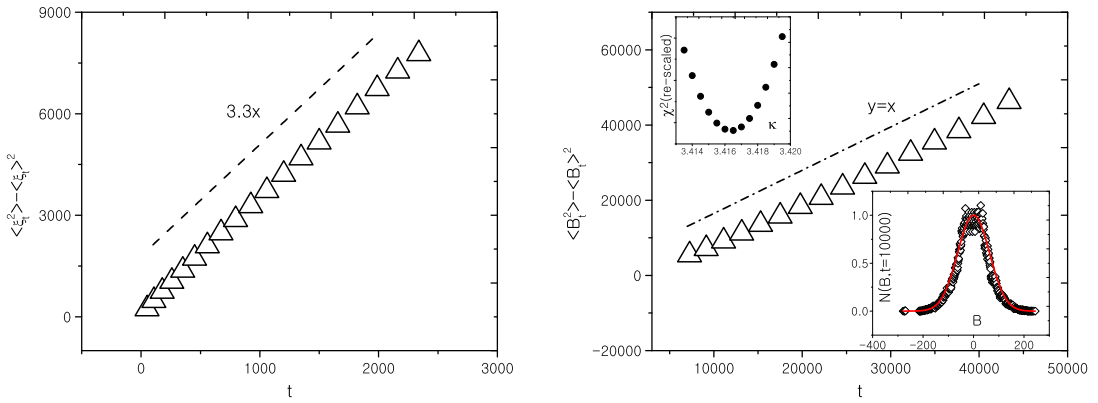

FIG. 8. (a) $\langle \zeta_t^2 \rangle - \langle \zeta_t \rangle^2$ in terms of t for the strip geometry. The slope, which is the diffusivity parameter, is $\kappa = 3.3 \pm 0.2$. (b) $\langle B_t^2 \rangle - \langle B_t \rangle^2$ in terms of t for the upper half-plane. The upper inset shows χ^2, the minimum of which is at $\kappa \simeq 3.42$. Lower inset: the distribution of $B_{t=5000}$, fitted by $\exp[-\frac{B^2}{10\,000}]$.

in which z_j^i is the jth point of the trace after the ith map, i.e., $z_j^i = g_{t_i}^S \circ g_{t_{i-1}}^S \circ \cdots g_{t_2}^S \circ g_{t_1}^S(z_j)$.

For the strip geometry, the stochastic curves start from the lower boundary and end on the upper boundary, as indicated in Fig. 7(a). In this paper, the ASYNNNI model is simulated on the $L_x \times L_y$ lattice in which $L_x = 1200$ and $L_y = 400 = \frac{L_x}{3}$ and the minimum length is considered to be $l_{\min} = 4000$. To avoid the possibility of crossing the vertical boundaries, $x = 0$ and $x = L_x$, the staggered spin on these boundaries is considered to be (+). To force a curve to start from the lower boundary ($y = 0$), we imply the boundary change in a random point on this line and let the upper boundary be open.

B. Real-axis-to-real-axis curves; SLE(κ,$\kappa - 6$)

Now consider a curve that starts from the origin and ends on a point on the real axis (x_∞). For the *real-axis-to-real-axis curves*, starting from the origin and ending on a point on the real axis (x_∞), using the map $\phi(z) = x_\infty z/(x_\infty - z)$, one can send the end point of the curve to infinity. This procedure leaves the equation for $g_t(z)$ unchanged, but it leads the drift term to acquire a drift term: $d\zeta_t = \sqrt{\kappa} dB_t + \frac{\kappa - 6}{\zeta_t - g_t(x_\infty)} dt$ [29,32]. As before, we uniformize curves by a composite map, each of which is defined by the slit map [33]. To generate the real-axis-to-real-axis random curves, the boundary conditions at two points x_0 and x_∞ should be changed, as is shown in Fig. 7(b). One has to discretized the equations as mentioned in the previous section by assuming the driving function to be piecewise constant (ζ_n) in some discrete time intervals $[t_{n-1}, t_n)$. Using the composite map $g_{\delta t_{n-1}, \zeta_{n-1}} \circ g_{\delta t_{n-2}, \zeta_{n-2}} \cdots \circ g_{t_0, \zeta_0}$ in which $\delta t_n \equiv t_n - t_{n-1}$, one can send every point on the SLE trace γ_t to the real axis step by step, in which $g_{\delta t_n, \zeta_n}(z) = \zeta_n + \sqrt{(z - \zeta_n)^2 + 4\delta t_n}$ [33,34]. The discretized driving function satisfies the relation $\frac{\zeta_n - \sum_{i=1}^{n} [\frac{\rho_c \delta t_i}{\zeta_i - G_{t_i}(x_\infty)}]}{\sqrt{\kappa}} = B_n$. After extracting ζ_t, the above equation is employed to yield the value of the diffusivity parameter, demanding the stochastic process on the right-hand side of this equation to be a 1D Brownian motion. The best fit to the Brownian motion gives us the value of κ. For this, we used the maximum-likelihood estimation method, for which the best fit and its precision can be obtained by looking at the distribution of χ^2 [35]. For the Brownian motion, we should have $\langle B_t \rangle = 0$ and $\langle B_t^2 \rangle - \langle B_t \rangle^2 = t$, where $\langle\rangle$ is the ensemble average, and $N_t(B) \sim \exp(\frac{-B^2}{2t})$, in which $N_t(B)$ is the distribution function of B at time t. The results are shown in Fig. 8(b). Figure 8(a) shows the results for the strip geometry. In that case, we found that $\langle \zeta \rangle \simeq 0$, as expected. The slope of $\langle \zeta_t^2 \rangle - \langle \zeta_t \rangle^2$ in terms of t is equal to the SLE diffusivity parameter, i.e., $\langle \zeta_t^2 \rangle - \langle \zeta_t \rangle^2 = \kappa t$. As is depicted in the figure, $\kappa = 3.3 \pm 0.2$. The results for the upper half-plane geometry have been shown in Fig. 8(b), which yields $\kappa = 3.42 \pm 0.2$. In the lower inset, we have shown the distribution for $B_{t=5000}$, which is properly fitted to $\exp[-\frac{B^2}{10^4}]$, indicating that $B(t)$ is fitted properly by one-dimensional Brownian motion. The results have been gathered in Table III.

VII. CONCLUSION

In this paper, we have investigated the tetragonal-orthorhombic (T-OII) structural phase transition of Y123 compounds. Toward that end, we mapped the system to the ASYNNNI model to capture the dynamics of oxygen atoms in the basal plane. After constructing the model by calculating the coupling constants, we employed the METROPOLIS and Wolff's (in the critical regions) Monte Carlo calculations to investigate the nature of this phase transition. The coupling constants of this dual model have been obtained using *ab initio* density-functional-theory calculations. In the first part

TABLE III. The exact κ value for the exterior perimeter of the geometrical spin clusters of the Ising and three-state Potts models [21,36,37] and the numerical result for the ASYNNNI model. c denotes the central charge in CFT.

	Ising	Three-state Potts model	ASYNNNI
κ	3	10/3	3.4 ± 0.2 [SLE(κ,$\kappa - 6$)] 3.3 ± 0.2 (strip mapping)
c	1/2 ($m = 3$ CFT)	4/5 ($m = 5$ CFT)	0.78

of the paper, we calculated and analyzed the local exponents of, e.g., critical heat capacity and staggered magnetization. The results show degrees of similarities with the three-state Potts model, as well as the ordinary Ising model. To be more precise, we calculated the geometrical statistical observables, e.g., the fractal dimension of the perimeter of geometrical spin clusters of the ASYNNNI model, the distribution of loop lengths, and their gyration radius. Results have been presented in Table II in comparison with the three-state Potts model and the Ising model. It was revealed that, with the magnetic transition in the ASYNNNI model, there occurs a percolation transition whose exponent has also been reported in this table. A comprehensive Schramm-Loewner evolution (SLE) analysis was performed on the interfaces of the model. Two geometries were chosen to test the SLE, i.e., the strip and the upper half-plane geometries. The diffusivity parameter for the geometrical spin clusters is found to be $\kappa = 3.3 \pm 0.2$, as is represented in Table III.

ACKNOWLEDGMENTS

We thank the anonymous referees for their helpful comments and detailed analysis.

[1] J. Chang, E. Blackburn, A. T. Holmes, N. B. Christensen, J. Larsen, J. Mesot, R. Liang, D. A. Bonn, W. N. Hardy, A. Watenphul, M. v. Zimmermann, E. M. Forgan, and S. M. Hayden, Nat. Phys. **8**, 871 (2012).

[2] J. Gomez del Campo, R. A. Dayras, J. A. Biggerstaff, D. Shapira, A. H. Snell, P. H. Stelson, and R. G. Stokstad, Phys. Rev. Lett. **43**, 26 (1979).

[3] D. J. Pringle, G. V. M. Williams, and J. L. Tallon, Phys. Rev. B **62**, 12527 (2000).

[4] A. Tavana, M. Akhavan, and C. Draxl, Physica C **517**, 20 (2015).

[5] N. H. Andersen, B. Lebech, and H. F. Poulsen, R. Hadfield, H. Casalta, N. H. Andersen, H. F. Poulsen, M. von Zimmermann, J. R. Schneider, R. Liang, P. Dosanjh, and W. N. Hardy, Physica C **172**, 31 (1991); P. Schleger, R. A. Hadfield, H. Casalta, N. H. Andersen, H. F. Poulsen, M. von Zimmermann, J. R. Schneider, R. Liang, P. Dosanjh, and W. N. Hardy, Phys. Rev. Lett. **74**, 1446 (1995).

[6] H. Lutgemeier and I. Heinmaa, in *Phase Separation in Cuprate Superconductors*, edited by K. A. Muller *et al.* (World Scientific, Singapore, 1993), p. 243.

[7] G. Campi, A. Ricci, N. Poccia, L. Barba, G. Arrighetti, M. Burghammer, A. S. Caporale, and A. Bianconi, Phys. Rev. B **87**, 014517 (2013).

[8] E. Blackburn *et al.*, Phys. Rev. Lett. **110**, 137004 (2013).

[9] M. Magnuson *et al.*, Sci. Rep. **4**, 7017 (2014).

[10] V. M. Matic *et al.*, J. Phys.: Condens. Matter **19**, 346230 (2007).

[11] D. de Fontaine, L. T. Wille, and S. C. Moss, Phys. Rev. B **36**, 5709 (1987).

[12] D. de Fontaine *et al.*, Nature (London) **343**, 544 (1990).

[13] V. M. Matic N. Dj. Lazarov, V. Spasojevic, M. Milic, and V. Kusigerski, Physica C **421**, 49 (2005).

[14] N. H. Andersen, M. von Zimmermann, T. Frello, M. Kall, D. Monster, P.-A. Lindgard, J. Madsen, T. Niemoller, H. F. Poulsen, O. Schmidt, J. R. Schneider, Th. Wolf, P. Dosanjh, R. Liang, and W. N. Hardy, Physica C **317**, 259 (1999).

[15] H. W. Seo, Q. Y. Chen, M. N. Iliev, T. H. Johansen, N. Kolev, U. Welp, C. Wang, and W. K. Chu, Phys. Rev. B **72**, 052501 (2005).

[16] P. Blaha *et al.*, *WIEN2k, An Augmented Plane Wave + Local Orbitals Program for Calculating Crystal Properties*, Karlheinz Schwarz (Techn. Universitat Wien, Austria).

[17] J. Hoshen and R. Kopelman, Phys. Rev. B **14**, 3438 (1976).

[18] P. A. Korzhavyi, C. Ambrocsh-Draxl, and B. Johansson, J. Low Temp. Phys. **117**, 395 (1999).

[19] B. Nienhuis, in Coulomb Gas Formulation of Two-dimensional Phase Transitions, in *Phase Transitions and Critical Phenomena*, edited by C. Domb and J. L. Lebowitz (Academic, New York, 1987), Vol. 11.

[20] F. Y. Wu, Rev. Mod. Phys. **54**, 235 (1982).

[21] J. Cardy, Ann. Phys. (NY) **318**, 81 (2005).

[22] M. P. M. Den Nijs, J. Phys. A **12**, 10 (1979).

[23] B. Nienhuis, E. K. Riedel, and M. Schick, J. Phys. A **13**, 189 (1980).

[24] E. Luijten and H. W. J. Blöte, Phys. Rev. B **56**, 8945 (1997); A. S. T. Pires, *ibid.* **53**, 5123 (1996); Z. Glumac and K. Uzelac, J. Phys. A **26**, 5267 (1993); S. A. Cannas, A. C. N. De Magalhaes, and F. A. Tamarit, Phys. Rev. B **61**, 11521 (2000).

[25] M. N. Najafi, S. Moghimi-Araghi, and S. Rouhani, Phys. Rev. E **85**, 051104 (2012).

[26] M. N. Najafi, Phys. Lett. A **380**, 370 (2016).

[27] G. Delfino, Nucl. Phys. B **818**, 196 (2009).

[28] O. Schramm, Isr. J. Math. **118**, 221 (2000).

[29] M. Bauer and D. Bernard, Commun. Math. Phys. **239**, 493 (2003).

[30] K. Kytola, J. Stat. Phys. **123**, 1169 (2006).

[31] D. Bernard *et al.*, Phys. Rev. B **76**, 020403 (2007).

[32] M. N. Najafi, Phys. Rev. E **87**, 062105 (2013); **92**, 022113 (2015).

[33] M. N Najafi, J. Stat. Mech. (2015) P05009.

[34] M. N. Najafi, S. Moghimi-Araghi, and S. Rouhani, J. Phys. A **45**, 095001 (2012).

[35] L. Le Cam, ISI Rev. **58**, 153 (1990).

[36] A. Gamsa and J. Cardy, J. Stat. Mech. (2007) P08020.

[37] P. Di Francesco, P. Mathieu, and D. Senegal, *Conformal Field Theory* (Springer, New York, 1997).